
IDENTIFYING AUTISM SPECTRUM DISORDER BASED ON INDIVIDUAL-AWARE DOWN-SAMPLING AND MULTI-MODAL LEARNING

A PREPRINT

Li Pan¹, Jundong Liu², Mingqin Shi³, Chi Wah Wong⁴, and Kei Hang Katie Chan^{1,2,5}

¹Department of Electrical Engineering, City University of Hong Kong, Hong Kong SAR

²Department of Biomedical Sciences, City University of Hong Kong, Hong Kong SAR

³School of Basic Medical Sciences, Yunnan University of Chinese Medicine, Kunming, China

⁴Department of Applied AI and Data Science, City of Hope, Duarte CA 91010, USA

⁵Department of Epidemiology, Brown University, Providence RI 02912, USA

ABSTRACT

Autism Spectrum Disorder(ASD) is a set of neurodevelopmental conditions that affect patients' social abilities. In recent years, deep learning methods have been employed to detect ASD through functional MRI (fMRI). However, existing approaches solely concentrated on the abnormal brain functional connections but ignored the importance of regional activities. Due to this biased prior knowledge, previous diagnosis models suffered from inter-site heterogeneity and inter-individual phenotypical differences. To address this issue, we propose a novel feature extraction method for fMRI that can learn a personalized low-resolution representation of the entire brain networking regarding both the functional connections and regional activities. First, we abstract the brain imaging as a graph structure, where nodes represent brain areas and edges denote functional connections, and downsample it to a sparse network by hierarchical graph pooling. Subsequently, by assigning each subject with the extracted features and building edges through inter-individual non-imaging characteristics, we build a population graph. The non-identically distributed node features are further recalibrated to node embeddings learned by graph convolutional networks. By these means, our framework can extract features directly and efficiently from the entire fMRI and be aware of implicit inter-individual differences. We have evaluated our framework on the ABIDE-I dataset with 10-fold cross-validation. The present model has achieved a mean classification accuracy of 85.95% and a mean AUC of 0.92, which is better than the state-of-the-art methods. Our code and support documents are available at: github.com/jhonP-Li/ASD_GP_GCN

Keywords ABIDE · Autism Spectrum Disorder · Graph Convolutional Networks · Graph Pooling

1 Introduction

Autism spectrum disorder (ASD), a range of brain developmental disorders, has been being commonly reported worldwide. In 2020, a survey found that approximately 1 in 45 children in the U.S. is diagnosed with this disease caused by genetic and environmental factors[1]. This mental disorganization, which will result in difficulties with social interaction and communication, can be noticed at the early age of a child. However, another study, done in the U.K., showed that the current diagnosis process was time-consuming and caused a delay of around 3.5 years from the point at which parents first consult a doctor to the confirmation of an ASD diagnosis[2], which results in unnecessary panic and late treatment.

Similar to physical disease diagnosis, this brain dysfunction can be detected with pathological manifestations. In [3], the authors proposed a diagnosis method based on the MRI of the brain. It was discovered that there existed structural differences in some certain areas between patients and typical control subjects. [4] reported abnormal brain function connections found on subjects with ASD. However, these diagnosis methods are too complex and specific to

be promoted as general ones. In recent years, brain imaging analysis based on deep learning and machine learning has been widely studied. [5] employed Long Short-Term Memory (LSTM) to automatically analyze the time-series data of fMRI. [6] applied Deep Neural Networks(DNN) directly on the fMRI and reported the performance improvement compared to Support Vector Machine (SVM) and Random Forest (RF). In [7], the authors designed a Convolutional Neural Networks (CNN) architecture with fMRI as input and achieved slightly better performance than the DNN did. [8] reached the best performance of end-to-end CNN models by 3D-CNN and ensemble brain atlas.

Limited by the number of available training data samples, trivial implementation of CNN models got stuck due to the high complexity of fMRI. The selection of abnormal brain functional connections has been commonly considered as a feasible solution. In [9], the authors noticed the importance of brain functional connections in this disease predicting and suggested 26.4 million possibilities among them. [10] extended the previous work by selecting the best framework from different brain region labeling and regional correlation computing methods. [11] directly downsampled the raw functional connections into the low-dimensional space by Principle Component Analysis(PCA). Yet, this straightforward dimension reduction method achieved even worse performance than the end-to-end models owing to the lack of samples. [12] reported the state-of-the-art performance by selecting features from brain functional connections. With the derived features, the model performance was improved even with a linear classifier. However, the specific feature selection workflow they proposed is not easy to be employed in other brain imaging feature selection problems. [13] compared two feature selection models, autoencoder and Multilayer Perceptron(MLP), which can automatically choose key features from the raw input. [14, 15] enhanced it with deep feature representation and multi-task feature selection respectively. Nevertheless, all the feature selection methods mentioned above concentrated on choosing the key components from the pairwise regional correlation matrix. These procedures considered only the correlations (edges) between every two brain regions but no regional activation information (nodes). At the same time, studies have found abnormal brain regional activities among ASD subjects[16, 17, 18, 19]. Thus, the improvement of the edge-only feature selection strategy could be expected if the nodes' information is also taken into consideration.

Widely employed in graph classification problems, graph pooling is used to downsample the whole graph structure. The intuitive pooling methods directly summed up or averaged all the node embeddings at the final layer [20]. In [21], the authors suggested a differentiable pooling method. By assigning nodes to clusters and replacing each cluster with a supernode repeatedly, the original graph is downsampled as one node. However, this procedure is not suitable for reasoning about the importance of different functional connections nor regional activities, because the nodes are coarsened as a logical supernode at each step. [22] improved it by ranking and selecting top-K nodes at each pooling layer at the price of losing graph information and isolating subgraphs. [23] presented a novel graph pooling method and achieved state-of-the-art performance on graph classification tasks. The pooling strategy they proposed downsamples the raw graph with the lowest information loss. Compared to the previous feature selection of functional connections, the graph representation of the brain imaging, downsampled by the graph pooling, has leveraged both the brain functional connections and regional signals.

In the context of this ASD disease prediction problem, another challenge is the non-imaging difference between individuals, i.e. gender, handedness, IQ, etc. Though this information is not present in the fMRI, it does affect the probability of someone suffering from ASD. For example, [24] indicated that One in every 42 males and one in 189 females in the United States is diagnosed with an autism spectrum disorder. [25] reported the correlations between handedness and ASD. Besides, the fMRI scanning devices and measurement parameters of different data collection sites are also different[12]. Those hidden factors have caused the non-identity distribution of features and affected the generalization of models. To address this, some authors manually kept those settings to be the same. For example, in [26, 27, 28, 29], the authors elaborately chosen training and testing samples from a certain data collection site. Hence, the implicit differences among samples were further narrowed and these methods achieved much better classification performance than the models evaluated on the entire dataset. Although the feasibility of ASD diagnosis based on deep learning has been proved in that way, this hard clustering strategy has reduced the number of available training and testing samples, so the model generalization ability could not be guaranteed.

To address the above issue, we employed Graph Convolutional Networks (GCN) to further redistribute the features extracted from brain imaging according to the non-imaging data. Unlike assigning each subject into a subset based on its non-imaging features, the soft clustering maintains a population graph for the entire dataset where the nodes denote subjects and edges indicate the non-imaging similarity between every two subjects. Thus, the phenotypic differences are represented implicitly as the internal and external connectivity differences among communities. Initially, the nodes are associated with features extracted from brain imaging by graph pooling as mentioned above. Then, the GCN, which extends the convolution operations to graph structures, is employed on the whole population graph. At each layer of GCN, the feature of each node is recalculated to the embeddings of the node's neighbors. With this differentiable node representation method, the features of subjects that are in the same community become more similar and the inter-community feature distribution differences become larger. In other words, the node features extracted from brain imaging are further recalibrated according to the inter-individual phenotypic variance. In [30], the authors employed

Table 1: Overview of the ABIDE I dataset preprocessed by CPAC

Sites	Age(year)		Gender		handedness				Diagnostic group	
	Min	Max	Male	Female	Left	Right	Ambi*	Mixed	ASD	Control
CALTECH	17.0	56.2	10	5	1	13	1	0	5	10
CMU	19.0	33.0	7	4	1	10	0	0	6	5
KKI	8.2	12.8	24	9	1	27	0	5	12	21
LEUVEN	12.1	32.0	49	7	7	49	0	0	26	30
MAX_MUN	7.0	58.0	42	4	2	44	0	0	19	27
NYU	6.5	39.1	136	36			N/A		74	98
OHSU	8.0	15.2	25	0	1	24	0	0	12	13
OLIN	10.0	24.0	23	5	5	23	0	0	14	14
PITT†	9.3	35.2	43	7	4	45	0	0	24	26
SBL†	20.0	49.0	26	0	1	0	0	0	12	14
SDSU	8.7	17.2	21	6	2	25	0	0	8	19
STANFORD	7.5	12.9	18	7	3	20	2	0	12	13
TRINITY	12.0	25.7	44	0	0	44	0	0	19	25
UCLA	8.4	17.9	74	11	9	76	0	0	48	37
UM†	8.2	28.8	93	27	15	97	0	0	47	73
USM	8.8	50.2	67	0			N/A		43	24
YALE	7.0	17.8	25	16	7	34	0	0	22	19
Total	6.5	58.0	727	144	59	531	3	5	403	468

* Ambi: Ambidextrous

† The handedness information of some subjects is unavailable.

GCN on the population graph for the first time and achieved performance improvement compared to end-to-end one-stage classifiers by leveraging imaging and non-imaging information. [31] extended the previous work by fusing both the MRI and fMRI into node features of the population graph. But it resulted in a lower accuracy owing to the increased model complexity.

In this study, we propose a novel framework that incorporates graph pooling and graph convolutional networks. We explicit graph pooling to leverage both the brain functional connections and regional signals, whereas previous methods solely selected several edges from that graph representation of the brain imaging. The selected brain substructures, which are flattened and then further regularized under inter-subject hidden factors to node embeddings learned through graph convolutional networks, preserve node-and-edge information and are clustering-like distributed in terms of phenotypical data. Having merged functional connections, regional activities, and non-imaging data, our framework presents its superior in ASD diagnosis, reaching an accuracy of 85.95% on ABIDE I dataset. The main contributions of our work are four-fold:

- 1) We have employed a novel feature extraction method on fMRI feature extraction tasks. The unsupervised graph pooling works without a strong assumption about specific brain functions and hence is flexible to be generalized to brain imaging downsampling problems. By weighing both the functional connections and regional signals at the same time, this efficient feature extractor has achieved promising performance in identifying brain disorders even with a linear classifier.
- 2) We have fused the multi-modal information through graph convolutional networks and intuitively illustrated its efficiency. This step successfully further stabilized the model classification performance by recalibrating extracted features according to non-imaging information.
- 3) Different from hard selecting universal biomarkers of ASD, our framework tends to select a sparse feature for individual brain imaging. This novel strategy has detected inter-group heterogeneity and intra-group homogeneity regarding brain activities.
- 4) We have constructed an ASD diagnosing framework, which outperforms state-of-the-art methods on the ABIDE I dataset, reaching a classification accuracy is improved to 85.95%. This clinically meaningful automatic ASD identification method could contribute to early detection and intervention for this brain disorders.

The rest of the paper is organized as follows: Section II introduces the datasets and illustrates the details of the proposed model. In Section III, we present the experimental setup, evaluation metrics, experimental results and comparison

with other methods, ablation study, and intuitive exhibition of model mechanisms. Finally, we draw the conclusion in Section IV.

2 Materials and Methods

2.1 ABIDE Dataset

Constructed by [32], the ABIDE I dataset contains a variety of information of 1,112 subjects, i.e. MRI, fMRI, and phenotype data, collected from 17 international sites. To reduce the measurement error, current researches are focusing on the preprocessed data. [33] performed four different preprocessing pipelines on the original material. To compare with the results of other methods [13, 12, 6, 8, 9], in the current paper, we used the data preprocessed by the Configurable Pipeline for the Analysis of Connectomes (CPAC). Built by [33], the chosen functional preprocessing pipeline includes time slicing, motion correction, skull-stripping, global mean intensity normalization, and nuisance signal regression. Thus, the noise caused by unrelated motions, like the heart beating, is reduced. To regularize the input sample features, band-pass filtering and global signal regression are also employed in this experiment.

As shown in the table 1, the processed data contains 403 ASD subjects and 468 typical control subjects. Caused by the measurement difference among different sites, some categories of the phenotype data are not or partially collected, like handedness information. Moreover, the distribution of the dataset is unbalanced on some features. For example, the 17 sites only have collected 144 female samples but collected 727 male samples. According to the view of [24], gender is a rather important factor affecting the probability of ASD. This unbalanced feature distribution, which is not present in the MRI or fMRI data, has caused the non-identical distribution of features and thus affected the performance of unimodal learning models.

To further reduce the dimensionality of input data, fMRI is separated logically as signals of regions of interest (ROIs). The voxel-wise time series is thus paraphrased as the time series of regional signals. Proposed by [34, 35, 36, 37], the Harvard-Oxford atlases is split into cortical and subcortical structural probabilistic atlases. The HO atlases, which has also been selected by other works[8, 13, 6], are filtered with a 25% threshold and subsequently divided into left and right hemispheres at the midline. The ROIs represent 110 functional brain regions, i.e., left and right Hippocampus, left and right Cuneal Cortex, left and right Planum Temporale, left and right Occipital Pole, etc. Thus, the original 4D brain imaging is further downsampled to a 2D data structure, containing 110 regions and the corresponding time series for each region.

2.2 Model Overview

As shown in the figure 1, the whole pipeline consists of three main parts. First, the unsupervised graph pooling directly downsamples the graph representation of the brain to a sparse brain networking. A multilayer perceptron is then trained using the flattened selected substructures and ground truth labels. Finally, by assigning every node in the population graph with further learned features, we train a two-layer graph convolutional networks model to learn the node embeddings with phenotypical information. After all the steps, the final node embeddings, which are fed into a sigmoid layer to predict the diagnostic label, have leveraged brain functional connections, regional activities, and non-imaging information.

2.3 Graph Pooling

In this section, we implement the Hierarchical Graph Pooling with Structural Learning presented by [23] to extract the features from the fMRI. It improves the existing brain imaging feature extractors in two main aspects. First, it can extract features directly from the entire graph structure, while other methods can only extract features from functional connections. Second, this graph pooling operation downsamples graph without supervision. In other words, this step can be directly added to other related frameworks without any additional training cost. Graph pooling, as a downsampling method for graph structure, is a central component of graph convolutional networks in graph classification tasks. For example, the intuitive idea is to average all node embeddings to represent the entire graph[20]. Compared to other graph pooling methods[21, 22], the HGP-SL is designed to preserve as much information as possible and reduce the information redundancy. Having achieved the state-of-the-art performance on graph classification problems, this method is suitable and efficient to extract the information from graph structures.

Before this implementation of graph pooling, other models trained classifiers, like MLP, or constructed a specific feature extracting framework to extract features from the functional connections[13, 14, 15, 12]. The functional connections are represented as the correlation coefficients of every two regions. During this stage, the details of the time series of regional activities are omitted. This intuitive method, mapping the two vectors to a float ranging from -1 to 1,

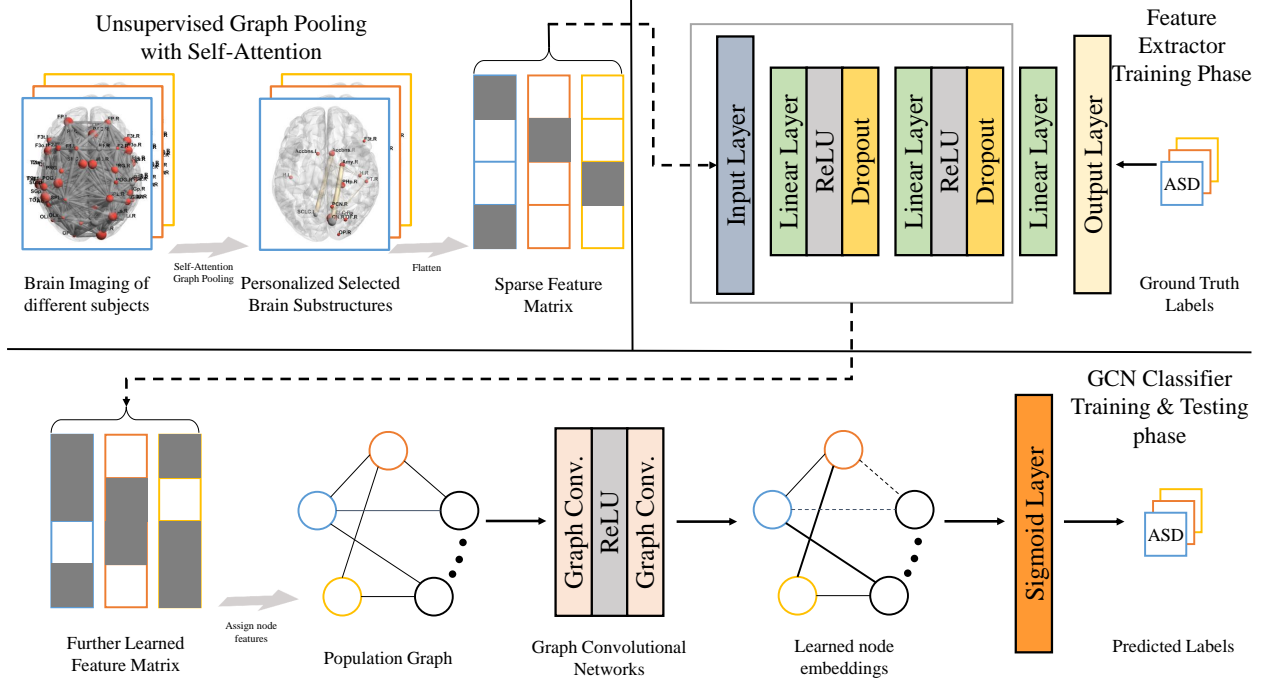


Figure 1: Overview of the proposed framework; The top-left part illustrates self-attention graph pooling in section 2.3. The top-right part indicates the training phase of feature extractor, where we train the MLP using the pooling output. In the bottom part, we construct a population graph, where nodes denote subjects and edges represent interindividual phenotypic similarity. We then train a GCN model by assigning each node with dense features extracted by MLP.

does reduce the data complexity. However, regarding the time series of brain regions as node features and functional connections as edges, this edge-only feature extraction strategy has caused much more information loss of the entire graph structure. Moreover, studies have proved the importance of the node features in the diagnosis of ASD. In [16, 17, 18, 19], the authors reported the abnormal regional activities found among ASD subjects. Thus, the graph pooling which considers both the node features and edges is a better choice.

2.3.1 Graph Representation of Brain Imaging

After being labeled as 110 regions according to the HO atlases, fMRI can be abstracted as a graph structure, where nodes denote brain regions and edges indicate functional connections. Initially, every node is assigned with a feature vector that represents the time series of regional activity. In [13], the authors defined 6105 brain functional connections by connecting right-side regions to the left side and left-side regions to the right. Inspired by it, we construct a graph representation of brain imaging, where regions are connected according to the same strategy and all regions are connected with the global mean time series to further reduce measurement error. In short, the input graph representation of brain imaging containing 111 nodes, 110 for the brain regions and 1 for the fMRI background, and 6215 edges.

2.3.2 Node Selection

The hierarchical graph pooling consists of two parts: First, it selects the nodes based on the criterion of minimizing graph information loss. Subsequently, to connect the probably isolated subgraph caused by the node selection and recorrect the initial brain regional connections to some degree, the edge prediction method is employed between the two-hop neighbors of each node and itself. At the first component, a node information score is defined as the absolute value of the Manhattan distance between the node features itself and the one constructed from its neighbors:

$$S = \gamma(g) = \left\| (I - (D^{(l)})^{-1}A^{(l)})H^{(l)} \right\|_1 \quad (1)$$

where $A^{(l)}$ and $H^{(l)}$ are the adjacency and node features matrices of the l -th layer. The information of edges is present implicitly as the connections among nodes. I represents the identity matrix and $D^{(l)}$ denotes the l -th layer diagonal degree matrix of $A^{(l)}$. $\|\cdot\|_1$ performs the \mathcal{L}_1 norm row-wisely. The vector S contains the information score of each

node, which indicates its importance at this selection stage. The nodes are then selected by ranking and selecting the top-K ones regarding the information score:

$$\begin{aligned} idx &= \text{top}(S, \lceil r * n^{(l)} \rceil) \\ H^{(l+1)} &= H^{(l)}(idx, :) \\ A^{(l+1)} &= A^{(l)}(idx, idx) \end{aligned} \quad (2)$$

where r is the pooling ratio which is set manually and will be discussed in the section 3.3. The function $\text{top}(\cdot)$ returns the indices of top $n^{(l+1)} = \lceil r * n^{(l)} \rceil$ values of the information scores S . $H^{(l)}(idx, :)$ and $A^{(l)}(idx, idx)$ performs the element selection according to the indices of top information scores. Thus, in the l -th layer, $n^{(l+1)}$ nodes are remained and others are removed.

Intuitively, the information score of a node is the feature difference between the average value of its neighbors and itself. The greater the difference, the higher the information score, and the less likely to remove the node. For example, if the feature of a node is equal to the average feature of its neighbors, it may be safe to drop this node without further information loss to the entire graph. On the other side, this selection method simulates a probable universal strategy for removing the information redundancy of fMRI: If the blood oxygen level activity of a region is close to it of its neighbors, the region may be regarded as coactivated with its neighbors. Removing all those nodes, the remained ones may be those that are activated in the first order, which may act like a trigger that has launched the sequence of brain regional activities.

2.3.3 Edge Prediction

At the same time, the node selection method may isolate some subgraphs and be sensitive to the initialization of brain graph structure, as it can not learn new connections beyond the given ones. To preserve the completeness of the graph, [23] developed a structural learning method that learned sparse graph structure through a sparse attention mechanism. Proposed by [38], the underlying pairwise relationship between disconnected nodes can be represented as the following:

$$\sigma^{(l)}(p, q) = \text{ReLU}(\vec{a}[H^{(l)}(p, :)||H^{(l)}(q, :)]^T) \quad (3)$$

where $H^{(l)}$ represents the feature matrix at the l -th layer. Thus, a similarity-like value is learned through the features of the two nodes. By adding a bias factor to keep a relatively large similarity to the connected nodes, the similarity score between two nodes can be measured as the follows:

$$\begin{aligned} E^{(l)}(p, q) &= \sigma^{(l)}(p, q) + \lambda \cdot A^{(l)}(p, q) \\ \text{Sim}^{(l)}(p, q) &= \frac{\exp(E^{(l)}(p, q))}{\sum_{m=1}^{n^{(l)}} \exp(E^{(l)}(p, m))} \end{aligned} \quad (4)$$

where $E^{(l)}(p, q)$ is the similarity score between the two nodes calculated by the attention mechanism. The bias $\lambda \cdot A^{(l)}(p, q)$ assigned a relatively larger similarity to the directly connected nodes. With normalized similarity values $\text{Sim}^{(l)}(p, q)$, this mechanism succeeded to predict the possible edges between disconnected nodes. Thus, the connectivity of the pooled graph is able to be preserved. Moreover, as shown in figure 4, this step is able to predict some connections that are not given in the initialization step, which makes the model more robust.

After three layers of graph pooling, the raw graph is downsampled to the sum-up of the three different hierarchical representations. The pooling output is then flattened and fed into a multilayer perception. At the training stage, we have employed a special procedure, i.e., we have run another 10-fold cross-validation on the given training folds and chosen the model that has been trained for at least 100 epochs and achieved the highest accuracy on the validation set to avoid overfitting and underfitting. After training, we remove the final linear layer and select the output feature map of the other two layers as the learned features, which will be discussed in section 2.4.

2.3.4 Personalized Feature Extraction

To conclude a universal ASD clinical diagnosis suggestion, [13, 14, 15, 12] tried to manually select top-N key functional connections from the fMRI of all subjects. Ideally, this procedure would return some functional connections from which we could easily tell if someone is suffering from this brain disorder. However, as discussed in [13], the results are not satisfactory: The highest mean accuracy is 70.40%, and the smallest number of selected functional connections is 250, which is not adequate nor efficient for clinical diagnosis.

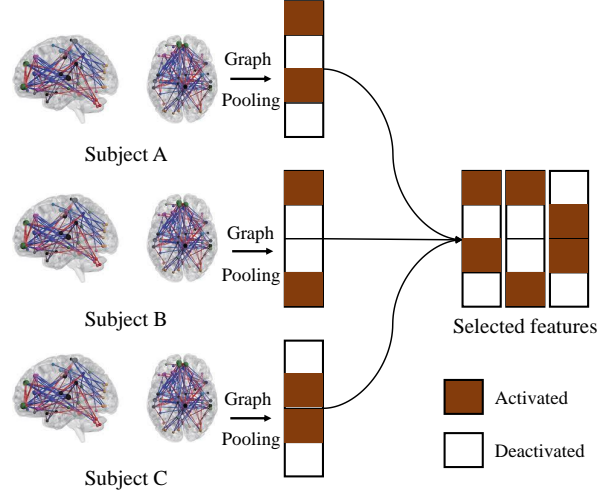


Figure 2: Illustration of sparse feature fusion in graph pooling

Different from that ambitious universal key features selection, we develop a personalized feature extraction strategy. Instead of selecting fixed connections or regions from brain imaging, we treat each subject separately and downsample the graph representation of brain imaging according to its own characters. As illustrated in the figure 2, the graph pooling result of each subject may be different and is stored as a sparse vector. For individuals, the features are successfully downsampled to a certain number of key components, just like the above feature selection. In terms of the extracted feature matrix of all subjects, the dimensionality is preserved, and the elements inside are sparsified. The two main benefits of this sparse feature fusion are as follows: First, it allows brain imaging to be downsampled to extraordinarily few key components even without a performance decrease. This will be discussed in the section 3.3. Second, the difference of selected features between individuals has clinical meanings. It may indicate the varied brain regional activities and connections among different groups and will be discussed in the section 3.4.

2.4 Graph Convolutional Networks

To fuse brain imaging data and non-imaging data, we constructed a population graph where nodes represent subjects and edges indicate the similarity degree regarding phenotypic information. The non-imaging information similarity among subjects is characterized as the connectivity degree among nodes, i.e. nodes with similar phenotypic properties are more likely to be in the same community. We employ Graph Convolutional Networks to process the population graph structure with every node associated with a feature vector extracted from its brain imaging by graph pooling. Proposed by [39], GCN extends convolution operations onto graph structures and is able to extract higher-order features from node embeddings. At each layer of GCN, the node feature vector is then recalculated as the lower-dimensional weighted sum of its and its neighbors' features, that is, the node embedding. Hence, the features of nodes that are in the same community tend to follow a similar distribution. A logistic regression classifier is trained on the final node features to predict the labels of each subject.

2.4.1 Population Graph Construction

As stated in section 2.1, we use the data of 871 subjects preprocessed by CPAC. The connection between two nodes is decided by their phenotypic similarity, i.e. gender, age, handedness, etc. However, caused by inconsistent measurement among different data collection sites, some categories of data are not or partly collected. For example, nearly 30% of the handedness data are not available as illustrated in the table 1. Suggested by [13], we consider a subset of the whole non-imaging data which contains gender, age, and data collection sites information. Intuitively, the similarity is computed as the cosine similarity between two phenotypic feature vectors M_u and M_v .

$$Sim(u, v) = \frac{M_u \cdot M_v}{\|M_u\| \|M_v\|} \quad (5)$$

Table 2: Comparison with state-of-the-art methods on ABIDE I dataset

References	Methods	Performance		
		Accuracy	Sensitivity	Specificity
[30]	GCN	69.50	-	-
[5]	LSTM	66.80	-	-
[10]	SVC	66.80	61.00	72.30
[6]	DNN	70.00	74.00	63.00
[13]	MLP and GCN	70.40	-	-
[8]	3D-CNN	73.30	-	-
[41]	Autoencoder	67.50	68.30	72.20
[12]	FCs selection and LDA	77.70	-	-
[42]	Joint learning	73.10	71.40	74.60
[7]	CNN	70.20	77.00	61.00
[15]	FCs selection and SVM	76.80	72.50	79.90
[14]	FCs selection and MLP	74.52	80.69	66.71
Present study	Graph pooling and LR	84.54	83.48	86.75
	Graph pooling and GCN	85.95	83.62	87.82

GCN: Graph Convolutional Networks
LSTM: Long Short-Term Memory
SVC: Support Vector Classification
MLP: Multi-Layer Perceptron
LDA: Linear Discriminant Analysis
LR: Logistic Regression
FCs: Functional Connections

where $M = \{Age, Gender, Site\}$ denotes the selected subset of non-imaging data. A threshold of 0.5 is then applied to the derived similarity values to decide whether the two nodes u, v are connected or not.

$$A(u, v) = \begin{cases} 1, & \text{if } Sim(u, v) > 0.5 \\ 0, & \text{otherwise} \end{cases} \quad (6)$$

where $Sim(u, v)$ is the similarity score of the two subjects. A represents the adjacency matrix of the graph. Two nodes are connected if their cosine similarity value is above 0.5. By these means, the population graph is initialized as an undirected graph containing 871 nodes.

2.4.2 GCNs

We have implemented two kinds of GCN in this part. The first layer is the same as the one proposed by [39]. The second layer is the Cluster-GCN presented by [40], which has accelerated the basic GCN block.

Extending convolution operations to non-Euclidean space, GCNs have achieved promising performance on arbitrarily structured graphs. Though there exist different forms of GCN block, the universal core task is to learn a non-linear function $f(H^{(l)}, A)$ which aggregates the feature vectors of connected nodes to generate features for next layer:

$$H^{(l+1)} = f(H^{(l)}, A) = \sigma(\tilde{D}^{-\frac{1}{2}} \tilde{A} \tilde{D}^{-\frac{1}{2}} H^{(l)} W^{(l)}) \quad (7)$$

with $\tilde{A} = A + I$, where I is the identity matrix and \tilde{D} is the diagonal node degree matrix of \tilde{A} . For the l -th layer of the GCN, the graph can be represented as the feature matrix $H^{(l)}$. $H^{(0)} = X$ and $H^{(L)} = Z$ denote the input and final output feature matrix respectively. $W^{(l)}$ is the learnable weight matrix and $\sigma(\cdot)$ is the non-linear activation function, ReLU. In this way, the features are aggregated to form features of the next layer. After the graph convolutional layers, a linear classifier is applied on each node. The final outputs of the classifier represent the probability of ASD. By filtering the probabilities with a 0.5 threshold, the model finally outputs the predicted diagnostic group of each subject.

$$P = \text{sigmoid}(H^{(L)}) \quad (8)$$

$$\text{Prediction}(sub_i) = \begin{cases} ASD, & \text{if } P(sub_i) \geq 0.5 \\ control, & \text{otherwise} \end{cases} \quad (9)$$

3 Experimental analysis

3.1 Experimental Settings

To make this experiment consistent with other studies [8, 12, 7, 13, 30, 5], the 10-fold cross validation is performed on the 871 samples and repeated 10 times. The graph pooling classifier and graph convolutional network is trained separately but on the same train set. The framework is trained on an NVIDIA TESLA V100S. During the optimization, the BCEloss is chosen as the loss function, and the Adam optimizer is employed of which the parameters are as follows: learning rate = 0.0001, weight decay = 0.01.

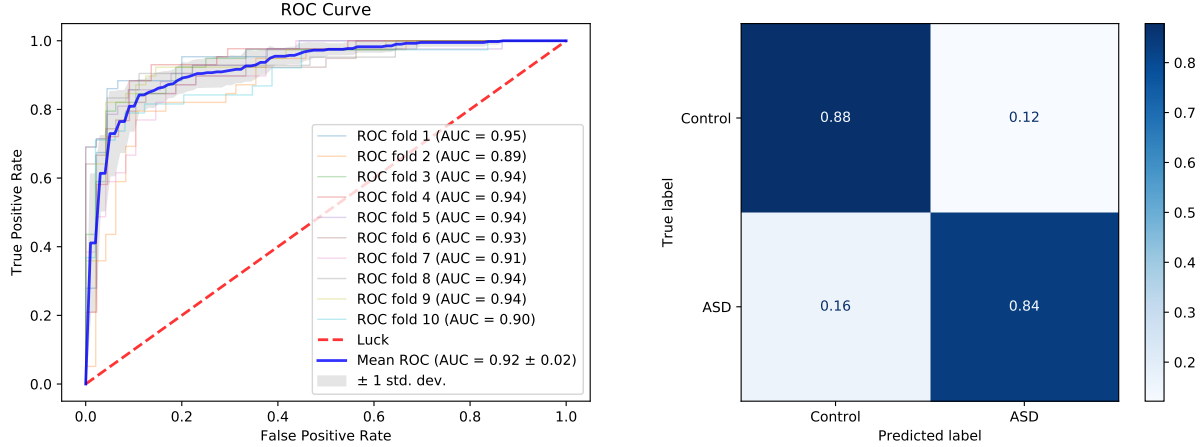


Figure 3: Performance of the present model, Graph pooling and GCN, on ABIDE I dataset: the ROC curve and confusion matrix

3.2 Results

In the table 2, we have compared our framework with other models on the same ABIDE I dataset preprocessed by CPAC [33]. In general, those methods can be categorized into two types: single-stage and multi-stage. The single-stage methods directly deploy deep learning methods, like CNN, to deal with this ASD VS Control binary image classification problem[5, 10, 6, 8, 41, 7]. However, limited by the number of available training samples, these naive implementations of neural networks have not achieved better performance for years. On the other hand, multi-stage methods usually consist of two components: feature extraction and classification. Previous works trained feature extractors to extract features from brain functional connections[13, 12, 15, 14]. A classifier, like SVC, is then trained with extracted features as inputs. This kind of framework has successfully downsampled the high-dimensional brain imaging and thus made obvious performance improvement even with linear classifiers compared to the straightforward CNN models. For example, [12] constructed a specific workflow to select the key features from brain imaging and achieved an accuracy of 77.7% with linear discriminant analysis.

The present framework includes feature extraction and classification parts like the above multi-stage methods. We implement graph pooling as a feature extractor that extracts features directly from the entire brain imaging. In the contrast, previous feature extractors can only extract features from brain functional connections. Inspired by [13], we employ GCN in the final classification part which can be aware of individual phenotypic differences. By these means, our framework outperforms the state-of-the-art method, reaching an accuracy of 85.95% and AUC of 0.92. The efficiency of graph pooling is discussed in the following part.

3.3 Efficiency of Graph Pooling

As previously mentioned, studies have reported abnormal brain functional connections found on ASD subjects[4]. With this prior knowledge, in [13, 12, 15, 14], the authors only simplified brain imaging as functional connections. Specifically, they computed correlation coefficients between every two regions and fed them into feature extractors. This correlation coefficient matrix representation of the brain successfully downsampled raw fMRI data, whereas it also resulted in key information loss as the regional features were omitted. In the contrast, the graph pooling extracts features directly from the graph representation of the brain. As shown in the table 3, graph pooling has outperformed the state-of-the-state method, reaching an accuracy of 84.54% even with linear regression as a classifier. Especially, in [10],

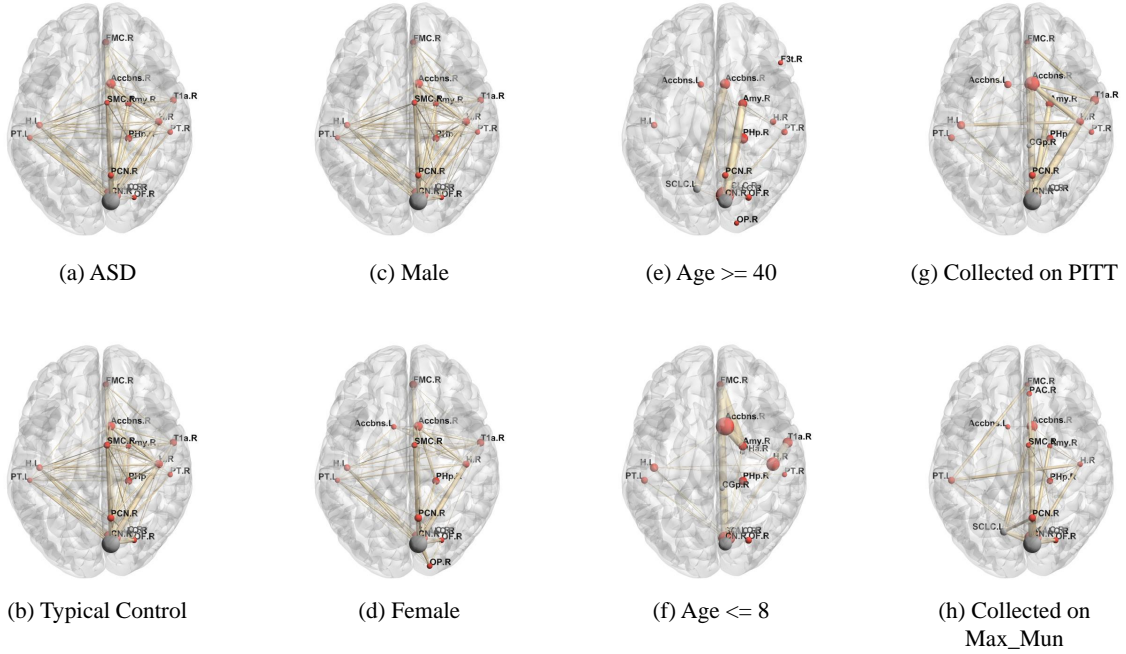


Figure 4: Result of graph pooling for different groups. The pooling ratio is set as 0.05, i.e., 6 regions are selected out of 111. Each axial view of the brain shows the top 15 nodes most frequently selected from those who are inside the corresponding group. The width of edges and size of nodes indicate the relative frequency of being selected. Number of subjects inside each group are as follows: a: 403; b: 468; c: 727; d: 144; e: 14; f: 15; g: 50; h: 46.

the authors have developed a similar workflow and achieved an accuracy of 66.80%. The only difference is that they extracted features from functional connections, whereas graph pooling downsamples the brain graph representation.

Table 3: The accuracy of ABIDE I classification with linear classifiers for different feature extraction methods

References	Feature extractor and classifier	Accuracy
[9]	FCs and SVC	60.00
[10]	MLP and SVC	66.80
[14]	FCs selection and MLP	74.52
[15]	FCs selection and SVM	76.80
Present study	Graph pooling and LR	84.54

To further evaluate the efficiency of graph pooling, we have tested the graph pooling progress for different values of the pooling ratio. Previous functional connection selection methods chose a certain number of edges from the graph representation of the brain [13, 12]. That inflexible strategy disregarded the heterogeneity of brain activities caused by inter-individual differences and even occasional personal status. Thus, that static procedure failed to achieve a satisfactory classification performance. As previously discussed in section 2.3.4, the self-attention mechanism inside graph pooling has realized personalized brain key components selections. Illustrated in figure 5, the classification of the framework is not sensitive to the super parameter, pooling ratio. The highest accuracy is even achieved with a pooling ratio of 0.005.

The main advantages of graph pooling are 3-fold: First, it can be easily generalized to other related problems. Previous methods work under a strong assumption that it is only the abnormal functional connections that cause ASD. This presupposition is not only biased in the current task [16, 17, 18, 19] but also limit generalizing these methods to other brain disorder diagnosing problems. On the contrary, graph pooling requires no prior knowledge about brain functions as it straight receives the entire graph representation of brain imaging. Besides, as discussed in section 2.3.2, this unsupervised downsampling method needs no training overhead. Second, it is more efficient for brain feature extraction. As shown in table 2, using features selected by graph pooling, a linear classifier can achieve much better performance

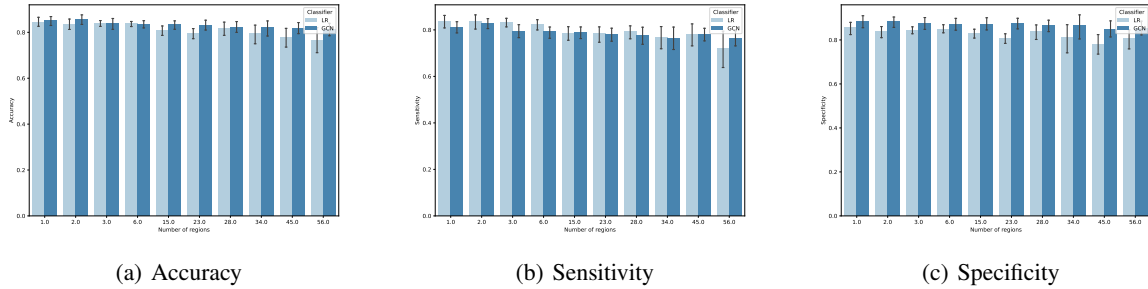


Figure 5: ABIDE I classification performance for the different numbers of brain regions selected at the graph pooling stage. Both the Logistic Regression and Graph Convolutional Networks work under the same settings.

than other more complex models did. In figure 5, we illustrate that the extracted features are still reliable even with the whole brain imaging downsampled to several nodes. Third, it can be aware of individual characters to some degree. This is benefited from the self-attention mechanism and sparse representation of extracted features, as discussed in section 2.3.4. We have observed differences in brain imaging pooling results of subjects from different groups, as shown in figure 4, and found even more obvious variance when we further split the groups.

3.4 Key Brain Substructures

Interpreting the ASD diagnosis framework has been being a hot topic as it may indicate the brain biomarkers of autism spectrum disorder and direct the early intervention. To intuitively exhibit the pooling results, i.e., the most important substructures selected at that stage, we have plotted them by BrainNet Viewer proposed by [43]. We have applied graph pooling onto the brain imaging of all subjects with a pooling ratio of 0.05. Thus, for every individual, the pooling result is 6 selected nodes and their connections. Subsequently, we have split 871 subjects into different groups regarding their non-imaging properties, including age, gender, and the data collection site they belong to. For each group, we have surveyed the top 15 most frequently selected regions and connections, from the pooling results of all subjects inside this group.

Unlike figuring out universal brain biomarkers of ASD, the outputs of self-attention pooling only have specified the importance of regions and edges of individual brain imaging. However, some conclusions can still be drawn by summarizing the pooling results in different groups. The illustrated substructures of the brain, as shown in figure 4, may indicate a common brain activity mechanism inside a certain group.

Ideally, as discussed in section 2.3.2, the remained regions are the first activated ones regarding external stress or active internal activities. They act like a trigger that has launched a sequence of regional activities. Based on this knowledge about model working principles, we have observed some inter-group heterogeneity in terms of key substructures selected by graph pooling. That finding indicates that self-attention graph pooling along can be aware of individual phenotypical properties to some degree. In figure 4, few differences have been found between ASD and Typical Control subjects as the heterogeneity caused by individual characteristics may be averaged. We further divide the two groups into four by incorporating gender into consideration, as shown in figure 6. According to the basic settings above, we may not draw a conclusion that it is the illustrated brain key substructures differences between different groups that have caused ASD.

3.5 Efficiency of Graph Convolutional Networks

In [13], the authors incorporated graph convolutional networks with brain functional selections and obtained accuracy improvement compared to [10]. The classification accuracy was increased from 66.80% to 70.40% by leveraging both imaging and non-imaging information with GCN. To figure out the efficiency of GCN in our framework, we have compared it with Logistic Regression under 10-fold cross-validation with the same dataset splits. As indicated in figure 5, the two classifiers, GCN and LR, have reached the highest accuracy when the pooling ratio is set as 0.01 and 0.005, respectively. Herein, we have followed that observation and without changing other settings.

Figure 7 indicates the classification accuracy differences between the two classifiers in terms of varied folds. Both two lines have shown the sensitivity to different training and testing datasets. To further discuss this impact of fold choice, we evaluate GCN and LR by changing graph pooling parameters. Like previously discussed, GCN should be able to further recalibrate the extracted features under the population graph. This regularization impact can be observed in



(a) Male ASD

(c) Male Typical Control



(b) Female Typical Control

(d) Female ASD

Figure 6: Additional brain view for figure 4 with same settings. The illustrated subgraphs indicate selection preference in graph pooling.

figure 8, i.e., when the training and testing sets are given, the performance of GCN is more stable compared to it of logistic regression. This assumption is also supported by the superior of GCN with regard to the standard deviation of both accuracy and AUC in table 4, which has been reported by [13, 30] as well.

Table 4: Compare classifiers: Linear Regression and Graph Convolutional Networks. The training overhead was calculated by training the both on one fold out of 10-fold cross-validation on an NVIDIA GTX1660 TI.

Measurement	Linear Regression	GCN
Mean Accuracy (%)	84.54	85.95
Standard Deviation of Accuracy	0.055	0.027
Area Under the ROC Curve	0.90	0.92
Standard Deviation of AUC	0.04	0.02
Average Training Overhead (s)	0.25	243.26
Average Training Epochs	625	10000

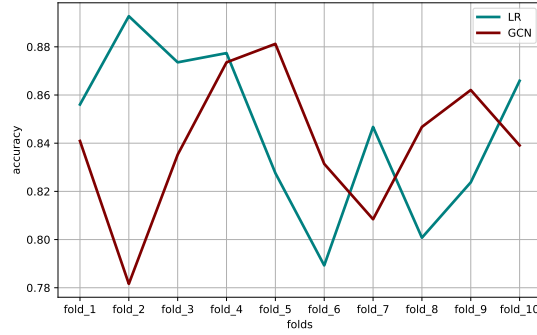


Figure 7: ABIDE I classification accuracy comparison between Linear Regression and Graph Convolutional Networks on 10 folds. Both the classifiers are trained using the same features extracted by graph pooling.

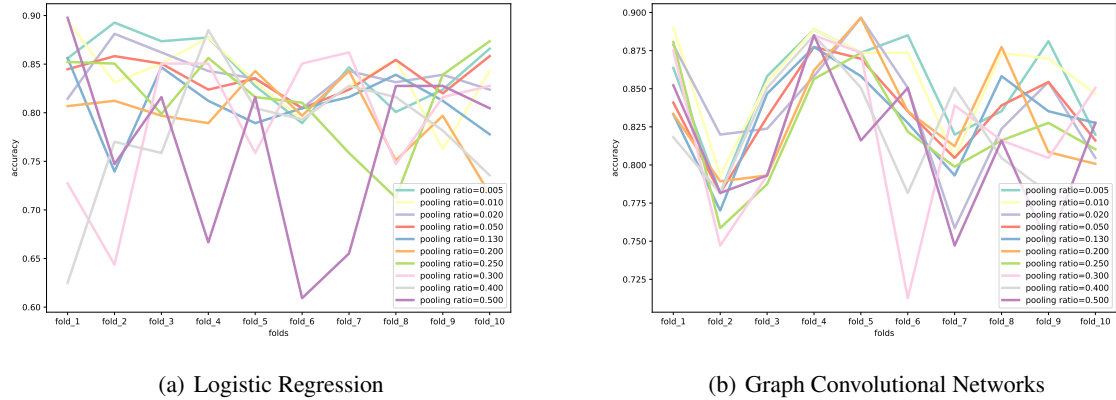
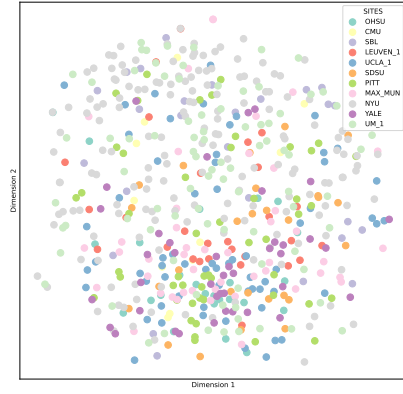


Figure 8: Impact of different folds for Logistic Regression and Graph Convolutional Networks

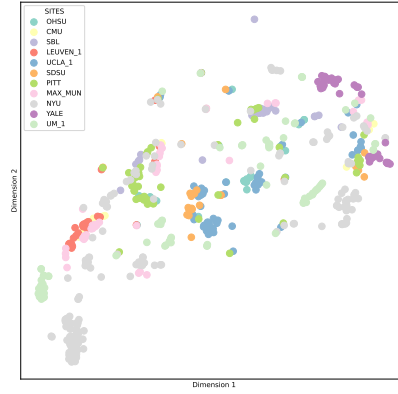
All the previous works, which have employed GCN for the same purpose of leveraging non-imaging information and fMRI [13, 30, 31], have assumed the ability of GCN to be aware of inter-individual phenotypical differences and to regularize raw features based on the former. Even though the regularization phenomenon is proved, to some degree, as discussed above, there is no clear conclusion that the GCN really has learned the inter-individual non-imaging differences. To intuitively present the learned node embeddings, we have downsampled them onto the 2D plane with t-SNE proposed by [44]. As shown in the left three plots of figure 9, even though graph pooling has detected some implicit inter-group heterogeneity, which is discussed in section 3.4, the features subsequently learned by MLP have not performed the relative feature distribution difference in respect of phenotypical information. The inevitable information loss during the feature dimensionality reduction may have caused this inconsistency, as the dimension of the raw features is up to 128. Still, the node embeddings learned by Graph Convolutional Networks have shown obvious clustering even in the 2D space. As exhibited in the right three diagrams of figure 9, the distance among subjects that are identical regarding a certain kind of phenotypical information is relatively close in the feature space compared to those who are not. This clustering is more obvious when only considering the genders, which indicates that the learned edge weights of the population graph may depend more on it.

4 conclusion

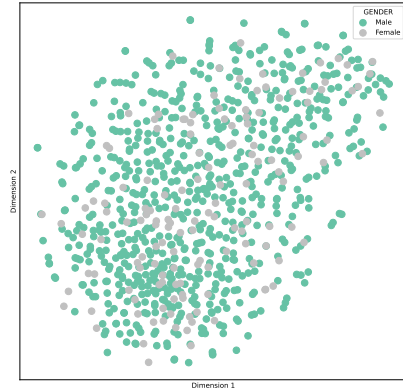
In this paper, we have proposed a framework for identifying Autism Spectrum Disorders. First, we have employed graph pooling to directly extract features from fMRI for the first time. This end-to-end, unsupervised, and flexible downsampling method successfully leverages brain functional connections and regional activities, and can be easily generalized to other brain imaging feature selection problems. Our framework has achieved a mean accuracy of



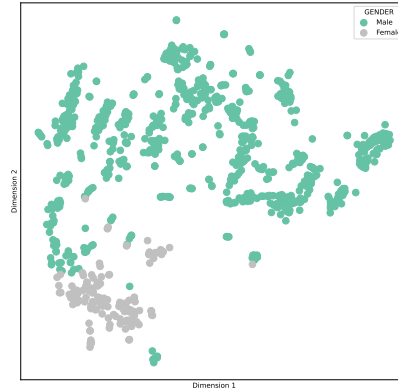
(a) Raw Extracted Features; Sites



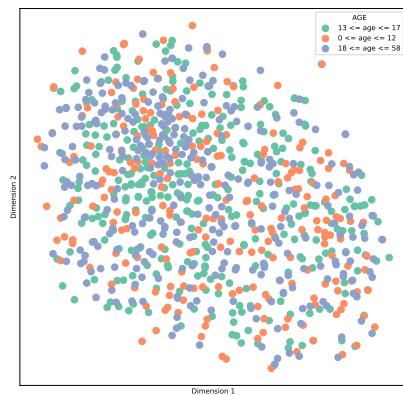
(b) Node Embeddings; Sites



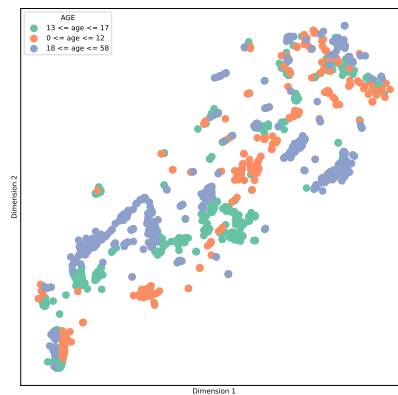
(c) Raw Extracted Features; Genders



(d) Node Embeddings; Genders



(e) Raw Extracted Features; Ages



(f) Node Embeddings; Ages

Figure 9: 2D view of the node embeddings learned by Graph Convolutional Networks. The nodes, which represent subjects, are colored according to different phenotypical properties: Sites, genders, and ages

85.95 \pm 0.03% and a mean AUC of 0.92 \pm 0.02 on ABIDE I dataset. The superior performance of our model indicates its ability to detect ASD and contribute to the early intervention.

References

- [1] M. J. Maenner, K. A. Shaw, J. Baio *et al.*, “Prevalence of autism spectrum disorder among children aged 8 years—autism and developmental disabilities monitoring network, 11 sites, united states, 2016,” *MMWR Surveillance Summaries*, vol. 69, no. 4, p. 1, 2020.
- [2] L. Crane, J. W. Chester, L. Goddard, L. A. Henry, and E. Hill, “Experiences of autism diagnosis: A survey of over 1000 parents in the united kingdom,” *Autism*, vol. 20, no. 2, pp. 153–162, 2016.
- [3] H. Oba, A. Yagishita, H. Terada, A. Barkovich, K. Kutomi, T. Yamauchi, S. Furui, T. Shimizu, M. Uchigata, K. Matsumura *et al.*, “New and reliable mri diagnosis for progressive supranuclear palsy,” *Neurology*, vol. 64, no. 12, pp. 2050–2055, 2005.
- [4] M. E. Villalobos, A. Mizuno, B. C. Dahl, N. Kemmotsu, and R.-A. Müller, “Reduced functional connectivity between v1 and inferior frontal cortex associated with visuomotor performance in autism,” *Neuroimage*, vol. 25, no. 3, pp. 916–925, 2005.
- [5] N. C. Dvornek, P. Ventola, K. A. Pelphrey, and J. S. Duncan, “Identifying autism from resting-state fmri using long short-term memory networks,” in *International Workshop on Machine Learning in Medical Imaging*. Springer, 2017, pp. 362–370.
- [6] A. S. Heinsfeld, A. R. Franco, R. C. Craddock, A. Buchweitz, and F. Meneguzzi, “Identification of autism spectrum disorder using deep learning and the abide dataset,” *NeuroImage: Clinical*, vol. 17, pp. 16–23, 2018.
- [7] Z. Sherkatghanad, M. Akhondzadeh, S. Salari, M. Zomorodi-Moghadam, M. Abdar, U. R. Acharya, R. Khosrowabadi, and V. Salari, “Automated detection of autism spectrum disorder using a convolutional neural network,” *Frontiers in neuroscience*, vol. 13, p. 1325, 2020.
- [8] M. Khosla, K. Jamison, A. Kuceyeski, and M. R. Sabuncu, “3d convolutional neural networks for classification of functional connectomes,” in *Deep Learning in Medical Image Analysis and Multimodal Learning for Clinical Decision Support*. Springer, 2018, pp. 137–145.
- [9] J. A. Nielsen, B. A. Zielinski, P. T. Fletcher, A. L. Alexander, N. Lange, E. D. Bigler, J. E. Lainhart, and J. S. Anderson, “Multisite functional connectivity mri classification of autism: Abide results,” *Frontiers in human neuroscience*, vol. 7, p. 599, 2013.
- [10] A. Abraham, M. P. Milham, A. Di Martino, R. C. Craddock, D. Samaras, B. Thirion, and G. Varoquaux, “Deriving reproducible biomarkers from multi-site resting-state data: An autism-based example,” *NeuroImage*, vol. 147, pp. 736–745, 2017.
- [11] A. Kazeminejad and R. C. Sotero, “The importance of anti-correlations in graph theory based classification of autism spectrum disorder,” *Frontiers in neuroscience*, vol. 14, p. 676, 2020.
- [12] S. Mostafa, L. Tang, and F.-X. Wu, “Diagnosis of autism spectrum disorder based on eigenvalues of brain networks,” *IEEE Access*, vol. 7, pp. 128 474–128 486, 2019.
- [13] S. Parisot, S. I. Ktena, E. Ferrante, M. Lee, R. Guerrero, B. Glocker, and D. Rueckert, “Disease prediction using graph convolutional networks: application to autism spectrum disorder and alzheimer’s disease,” *Medical image analysis*, vol. 48, pp. 117–130, 2018.
- [14] Y. Wang, J. Wang, F.-X. Wu, R. Hayrat, and J. Liu, “Aimafe: autism spectrum disorder identification with multi-atlas deep feature representation and ensemble learning,” *Journal of Neuroscience Methods*, p. 108840, 2020.
- [15] J. Liu, Y. Sheng, W. Lan, R. Guo, Y. Wang, and J. Wang, “Improved asd classification using dynamic functional connectivity and multi-task feature selection,” *Pattern Recognition Letters*, vol. 138, pp. 82–87, 2020.
- [16] A. A. Sáenz, M. Septier, P. Van Schuerbeek, S. Baijot, N. Deconinck, P. Defresne, V. Delvenne, G. Passeri, H. Raeymaekers, L. Salvesen *et al.*, “Adhd and asd: distinct brain patterns of inhibition-related activation?” *Translational psychiatry*, vol. 10, no. 1, pp. 1–10, 2020.
- [17] G. J. Harris, C. F. Chabris, J. Clark, T. Urban, I. Aharon, S. Steele, L. McGrath, K. Condouris, and H. Tager-Flusberg, “Brain activation during semantic processing in autism spectrum disorders via functional magnetic resonance imaging,” *Brain and cognition*, vol. 61, no. 1, pp. 54–68, 2006.
- [18] N. Hadjikhani, R. M. Joseph, J. Snyder, and H. Tager-Flusberg, “Abnormal activation of the social brain during face perception in autism,” *Human brain mapping*, vol. 28, no. 5, pp. 441–449, 2007.

- [19] S.-Y. Kim, U.-S. Choi, S.-Y. Park, S.-H. Oh, H.-W. Yoon, Y.-J. Koh, W.-Y. Im, J.-I. Park, D.-H. Song, K.-A. Cheon *et al.*, “Abnormal activation of the social brain network in children with autism spectrum disorder: an fmri study,” *Psychiatry investigation*, vol. 12, no. 1, p. 37, 2015.
- [20] D. Duvenaud, D. Maclaurin, J. Aguilera-Iparraguirre, R. Gómez-Bombarelli, T. Hirzel, A. Aspuru-Guzik, and R. P. Adams, “Convolutional networks on graphs for learning molecular fingerprints,” *arXiv preprint arXiv:1509.09292*, 2015.
- [21] R. Ying, J. You, C. Morris, X. Ren, W. L. Hamilton, and J. Leskovec, “Hierarchical graph representation learning with differentiable pooling,” *arXiv preprint arXiv:1806.08804*, 2018.
- [22] H. Gao and S. Ji, “Graph u-nets,” in *international conference on machine learning*. PMLR, 2019, pp. 2083–2092.
- [23] Z. Zhang, J. Bu, M. Ester, J. Zhang, C. Yao, Z. Yu, and C. Wang, “Hierarchical graph pooling with structure learning,” *arXiv preprint arXiv:1911.05954*, 2019.
- [24] R. Loomes, L. Hull, and W. P. L. Mandy, “What is the male-to-female ratio in autism spectrum disorder? a systematic review and meta-analysis,” *Journal of the American Academy of Child & Adolescent Psychiatry*, vol. 56, no. 6, pp. 466–474, 2017.
- [25] A. L. Rysstad and A. V. Pedersen, “There are indeed more left-handers within the autism spectrum disorder compared with in the general population, but the many mixed-handers is the more interesting finding,” *Journal of autism and developmental disorders*, vol. 48, no. 9, pp. 3253–3255, 2018.
- [26] X. Guo, K. C. Dominick, A. A. Minai, H. Li, C. A. Erickson, and L. J. Lu, “Diagnosing autism spectrum disorder from brain resting-state functional connectivity patterns using a deep neural network with a novel feature selection method,” *Frontiers in neuroscience*, vol. 11, p. 460, 2017.
- [27] Y. Kong, J. Gao, Y. Xu, Y. Pan, J. Wang, and J. Liu, “Classification of autism spectrum disorder by combining brain connectivity and deep neural network classifier,” *Neurocomputing*, vol. 324, pp. 63–68, 2019.
- [28] H. Li, N. A. Parikh, and L. He, “A novel transfer learning approach to enhance deep neural network classification of brain functional connectomes,” *Frontiers in neuroscience*, vol. 12, p. 491, 2018.
- [29] X.-a. Bi, Y. Liu, Q. Jiang, Q. Shu, Q. Sun, and J. Dai, “The diagnosis of autism spectrum disorder based on the random neural network cluster,” *Frontiers in human neuroscience*, vol. 12, p. 257, 2018.
- [30] S. Parisot, S. I. Ktena, E. Ferrante, M. Lee, R. G. Moreno, B. Glocker, and D. Rueckert, “Spectral graph convolutions for population-based disease prediction,” in *International conference on medical image computing and computer-assisted intervention*. Springer, 2017, pp. 177–185.
- [31] D. Arya, R. Olij, D. K. Gupta, A. El Gazzar, G. Wingen, M. Worrying, and R. M. Thomas, “Fusing structural and functional mris using graph convolutional networks for autism classification,” in *Medical Imaging with Deep Learning*. PMLR, 2020, pp. 44–61.
- [32] A. Di Martino, C.-G. Yan, Q. Li, E. Denio, F. X. Castellanos, K. Alaerts, J. S. Anderson, M. Assaf, S. Y. Bookheimer, M. Dapretto *et al.*, “The autism brain imaging data exchange: towards a large-scale evaluation of the intrinsic brain architecture in autism,” *Molecular psychiatry*, vol. 19, no. 6, pp. 659–667, 2014.
- [33] C. Craddock, Y. Benhajali, C. Chu, F. Chouinard, A. Evans, A. Jakab, B. S. Khundrakpam, J. D. Lewis, Q. Li, M. Milham *et al.*, “The neuro bureau preprocessing initiative: open sharing of preprocessed neuroimaging data and derivatives,” *Frontiers in Neuroinformatics*, vol. 7, 2013.
- [34] R. S. Desikan, F. Ségonne, B. Fischl, B. T. Quinn, B. C. Dickerson, D. Blacker, R. L. Buckner, A. M. Dale, R. P. Maguire, B. T. Hyman *et al.*, “An automated labeling system for subdividing the human cerebral cortex on mri scans into gyral based regions of interest,” *Neuroimage*, vol. 31, no. 3, pp. 968–980, 2006.
- [35] J. M. Goldstein, L. J. Seidman, N. Makris, T. Ahern, L. M. O’Brien, V. S. Caviness Jr, D. N. Kennedy, S. V. Faraone, and M. T. Tsuang, “Hypothalamic abnormalities in schizophrenia: sex effects and genetic vulnerability,” *Biological psychiatry*, vol. 61, no. 8, pp. 935–945, 2007.
- [36] N. Makris, J. M. Goldstein, D. Kennedy, S. M. Hodge, V. S. Caviness, S. V. Faraone, M. T. Tsuang, and L. J. Seidman, “Decreased volume of left and total anterior insular lobule in schizophrenia,” *Schizophrenia research*, vol. 83, no. 2-3, pp. 155–171, 2006.
- [37] J. A. Frazier, S. Chiu, J. L. Breeze, N. Makris, N. Lange, D. N. Kennedy, M. R. Herbert, E. K. Bent, V. K. Koneru, M. E. Dieterich *et al.*, “Structural brain magnetic resonance imaging of limbic and thalamic volumes in pediatric bipolar disorder,” *American Journal of Psychiatry*, vol. 162, no. 7, pp. 1256–1265, 2005.
- [38] A. Martins and R. Astudillo, “From softmax to sparsemax: A sparse model of attention and multi-label classification,” in *International conference on machine learning*. PMLR, 2016, pp. 1614–1623.

- [39] T. N. Kipf and M. Welling, "Semi-supervised classification with graph convolutional networks," *arXiv preprint arXiv:1609.02907*, 2016.
- [40] W.-L. Chiang, X. Liu, S. Si, Y. Li, S. Bengio, and C.-J. Hsieh, "Cluster-gcn: An efficient algorithm for training deep and large graph convolutional networks," in *Proceedings of the 25th ACM SIGKDD International Conference on Knowledge Discovery & Data Mining*, 2019, pp. 257–266.
- [41] T. Eslami, V. Mirjalili, A. Fong, A. R. Laird, and F. Saeed, "Asd-diagnet: a hybrid learning approach for detection of autism spectrum disorder using fmri data," *Frontiers in neuroinformatics*, vol. 13, p. 70, 2019.
- [42] H. Jiang, P. Cao, M. Xu, J. Yang, and O. Zaiane, "Hi-gcn: A hierarchical graph convolution network for graph embedding learning of brain network and brain disorders prediction," *Computers in Biology and Medicine*, vol. 127, p. 104096, 2020.
- [43] M. Xia, J. Wang, and Y. He, "Brainnet viewer: a network visualization tool for human brain connectomics," *PloS one*, vol. 8, no. 7, p. e68910, 2013.
- [44] L. Van der Maaten and G. Hinton, "Visualizing data using t-sne." *Journal of machine learning research*, vol. 9, no. 11, 2008.